

## Article

# Bio-Catalytic Activity of Novel *Mentha arvensis* Intervened Biocompatible Magnesium Oxide Nanomaterials

Shah Faisal <sup>1,\*</sup>, Abdullah <sup>2</sup>, Hasnain Jan <sup>1,3</sup>, Sajjad Ali Shah <sup>1</sup>, Sumaira Shah <sup>4</sup>, Muhammad Rizwan <sup>5</sup>, Nasib Zaman <sup>5</sup> , Zahid Hussain <sup>5</sup>, Muhammad Nazir Uddin <sup>5</sup>, Nadia Bibi <sup>6</sup> , Aishma Khattak <sup>7</sup>, Wajid Khan <sup>5</sup>, Arshad Iqbal <sup>5</sup>, Muhammad Idrees <sup>8</sup> and Rehana Masood <sup>9</sup>

- <sup>1</sup> Institute of Biotechnology and Microbiology, Bacha Khan University, Charsadda 24460, KPK, Pakistan; rhasnain849@gmail.com (H.J.); sajjadbiotec@gmail.com (S.A.S.)
- <sup>2</sup> Department of Microbiology, Abdul Wali Khan University, Mardan 23200, KPK, Pakistan; abdul.9353chd@gmail.com
- <sup>3</sup> Department of Biotechnology, Quaid-i-Azam University, Islamabad 45320, Pakistan
- <sup>4</sup> Department of Botany, Bacha Khan University, Charsadda 24460, KPK, Pakistan; sunehra23@gmail.com
- <sup>5</sup> Centre for Biotechnology and Microbiology University of Swat, Mingora 19200, KPK, Pakistan; muhammad.rizwan@uswat.edu.pk (M.R.); nasibzaman@uswat.edu.pk (N.Z.); zahid@uswat.edu.pk (Z.H.); nazir@uswat.edu.pk (M.N.U.); sherafghan.shah@gmail.com (W.K.); arshad.iqbal@uswat.edu.pk (A.I.)
- <sup>6</sup> Department of Microbiology, Shaheed Benazir Bhutto Women University, Peshawar 25000, KPK, Pakistan; nadiabibi@sbbwu.edu.pk
- <sup>7</sup> Department of Bioinformatics, Shaheed Benazir Bhutto Women University, Peshawar 25000, KPK, Pakistan; aishma.khattak@yahoo.com
- <sup>8</sup> Department of Biotechnology, University of Swabi, Swabi 23430, KPK, Pakistan; midrees@uoswabi.edu.pk
- <sup>9</sup> Department of Biochemistry, Shaheed Benazir Bhutto Women University, Peshawar 25000, KPK, Pakistan; rehana.masood@sbbwu.edu.pk
- \* Correspondence: shahfaisal\_std@bkuc.edu.pk; Tel.: +92-3159353867



**Citation:** Faisal, S.; Abdullah, Jan, H.; Shah, S.A.; Shah, S.; Rizwan, M.; Zaman, N.; Hussain, Z.; Uddin, M.N.; Bibi, N.; et al. Bio-Catalytic Activity of Novel *Mentha arvensis* Intervened Biocompatible Magnesium Oxide Nanomaterials. *Catalysts* **2021**, *11*, 780. <https://doi.org/10.3390/catal11070780>

Academic Editor: Beom Soo Kim

Received: 24 May 2021  
Accepted: 21 June 2021  
Published: 27 June 2021

**Publisher's Note:** MDPI stays neutral with regard to jurisdictional claims in published maps and institutional affiliations.



**Copyright:** © 2021 by the authors. Licensee MDPI, Basel, Switzerland. This article is an open access article distributed under the terms and conditions of the Creative Commons Attribution (CC BY) license (<https://creativecommons.org/licenses/by/4.0/>).

**Abstract:** In the present study *Mentha arvensis* mediated Magnesium oxide nanoparticles were synthesized by novel green route followed by advanced characterization via XRD, FTIR, UV, SEM, TEM, DLS and TGA. The mean grain size of 32.4 nm and crystallite fcc morphology were confirmed by X-ray diffractive analysis. Scanning and Transmission electron microscopy analysis revealed the spherical and elliptical morphologies of the biosynthesized nanoparticles. Particle surface charge of  $-16.1$  mV were determined by zeta potential and zeta size of 30–120 nm via dynamic light scattering method. Fourier transform spectroscopic analysis revealed the possible involvement of functional groups in the plant extract in reduction of  $Mg^{2+}$  ions to  $Mg^0$ . Furthermore, the antioxidant, anti-Alzheimer, anti-cancer, and anti-*H. pylori* activities were performed. The results revealed that MgO-NPs has significant anti-*H. pyloric* potential by giving ZOI of  $17.19 \pm 0.83$  mm against *Helicobacter felis* followed by *Helicobacter suis*. MgO-NPs inhibited protein kinase enzyme up to  $12.44 \pm 0.72\%$  at 5 mg/mL and thus showed eminent anticancer activity. Significant free radicals scavenging and hemocompatibility was also shown by MgO-NPs. MgO-NPs also displayed good inhibition potential against Hela cell lines with maximum inhibition of  $49.49 \pm 1.18$  at 400  $\mu$ g/mL. Owing to ecofriendly synthesis, non-toxic and biocompatible nature, *Mentha arvensis* synthesized MgO-NPs can be used as potent antimicrobial agent in therapeutic applications.

**Keywords:** *Mentha arvensis*; green synthesis; magnesium oxide; antibacterial; bio-compatible; anti-cancer

## 1. Introduction

Nanotechnology, with various branches rooted in industrial sector such as biomedical, nanomedicine, cosmetics, pharmaceutical, and food manufacturing, is now seen as an established, state of the art technology [1]. Many nano-scaled structures have been produced using various techniques. Yet the synthesis of green nanoparticles is a method of choice that is easy to plan and engineer [2]. Traditional approaches to nanoparticle development

have a number of drawbacks, including long-term processing, high prices, time-consuming methods, and the use of toxic compounds in particular. Because of these drawbacks, much of the relevant research has focused on developing environment friendly nanoparticles synthetic approach [3,4].

Plant mediated Synthetic methods that are less harmful to the environment are being created. In recent years, material scientists have prioritised the production of environmentally sustainable methods for synthesising nanoscale materials. Green NP synthesis, especially using various plant extracts, is an emerging field in trend in environment friendly chemistry and thought to be simple, inexpensive, and non-toxic [5–7]. Nanoscience has improved the human life by addressing a wide range of issues, and play an important role in treating many diseases [8,9]. Magnesium oxide nanoparticles has ionic properties with good crystal structure and has a vital role in novel applications such as adsorption, electronics, catalysis, and in extraction of petrochemicals [10–12]. It can be synthesized by different approaches but the green route is more advantageous. The physico-morphic properties i.e., size, shape and crystallinity of MgO nanoparticles depending on the reaction time and condition [13–15]. Material scientists are now using the enormous potentiality of medicinal plants as a reliable basis for the development of (MgO) nanoparticles as an alternative to traditional approaches, according to the aforementioned disadvantages of synthetic methods other than green.

*Mentha arvensis* is a 40-cm tall herbaceous plant with a pleasant, calming odour. Hortel-vick is the common name for it. It's used to treat skin infections and is prescribed as a gastrointestinal, carminative, and nasal decongestant in conventional medicine [16,17]. This species' essential oil is rich in menthol (70%) and is used in nasal inhalants, perfumes, tobacco, and the pharmaceutical industry. *Mentha arvensis* was found to contain menthol, -terpineol, p-menthone, menthol acetate, and other compounds [17]. UV spectroscopy, FTIR, XRD, SEM, TEM, DLS, EDX, and TGA were used to classify the bio-inspired synthesised MgO-NPs. Furthermore, inhibition of protein kinase enzyme, antidiabetic, anti-Alzheimer's, antimicrobial, antioxidant, and cytotoxic applications of the synthesised nanoparticles were assessed. Biocompatibility of MgO-NPs against human enterocytes were also tested to ensure the engineered nanoparticles are bio safe.

## 2. Results

### 2.1. Biosynthesis of MgO-NPs

*Mentha arvensis*, also known as "wild mint" and is used in drug production, it has a variety of pharmacological practises in different countries. They also contain therapeutic compounds that are well known for their medicinal properties, such as anti-inflammatory, antioxidant, and gastro protective properties [18]. HPLC studies have identified the most active compounds in *M. arvensis* extracts, including hesperidin, ferulic acid, rosmarinic acid, diosmin, didymin, buddleoside, acacetin, and linarin, and have reported a variety of biological effects. Rosmarinic acid, which is present in plants, has been studied for its antioxidant and anti-inflammatory properties [19,20]. As a reducing, capping, and stabilising agent, aqueous leaf extract of *M. arvensis* was used in the biosynthesis of MgO-NPs. The constituents contained in *M. arvensis* extracts are thought to have played a significant role in the production of environmentally sustainable and biomedically essential MgO-NPs. The colour of the mixture changes from light brown to darkish brown when the reaction between  $(\text{Mg}(\text{NO}_3)_2 \cdot 6\text{H}_2\text{O} + \text{M. arvensis})$  is carried out, confirming the development of MgO-NPs [20]. Figure 1. After Washing, drying, grinding, and calcination is followed by the development of a dark brown powder of MgO-NPs. The fine powder was extracted and deposited at room temperature in an airtight glass vial labelled MgO-NPs for physico-chemical, morphological, and biological applications. The results of the literature review showed that the physicochemical and morphological properties of metallic nanoparticles depends upon the type of plant and reaction conditions [21].

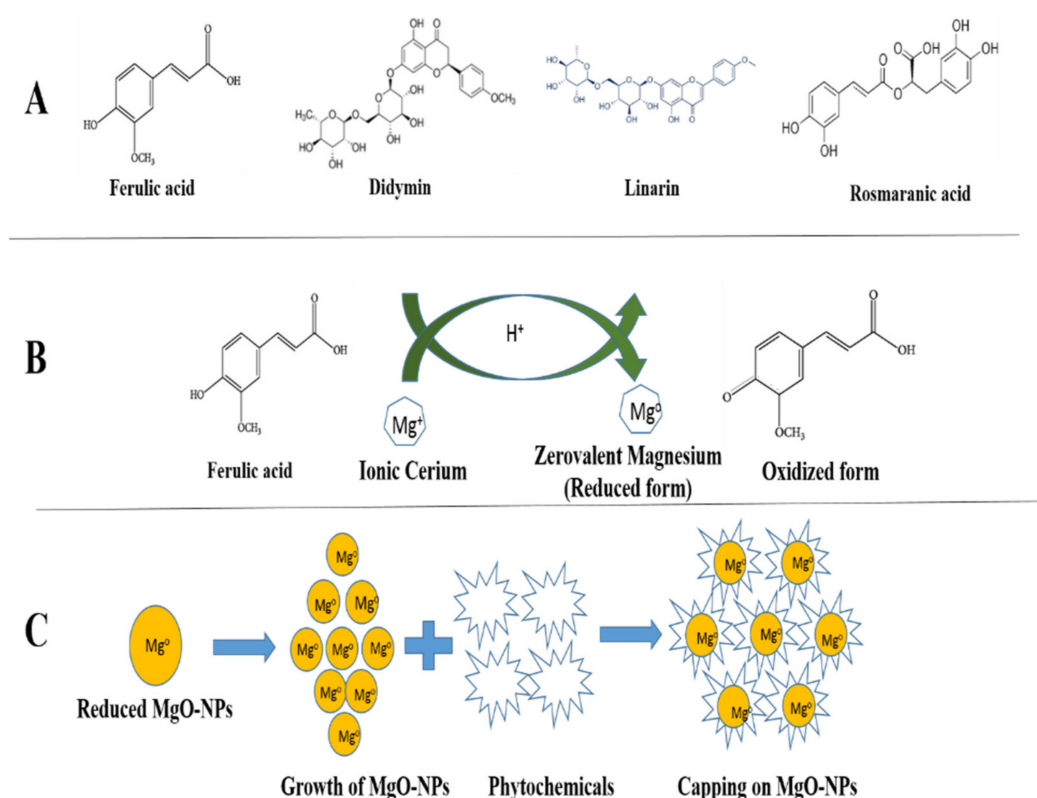


**Figure 1.** Mechanistic approach for synthesis of MgO-NPs using aqueous extract of *Mentha arvensis*. (A) The structural and chemical formulas of Ferulic acid, Didymin, Linarin, Rosmaranic acid these all compounds are present in *Mentha arvensis* extract. (B) Ferulic acid interacts with magnesium ion and reduced it to  $Mg^{+1}$  to  $Mg^0$ . (C) Reduced form of magnesium nanoparticles and phytochemicals that are taking part in in capping o magnesium nanoparticles.

## 2.2. Optical Band Gap

Figure 2a shows how the optical band distance of MgO nanoparticles was calculated using the simple relationship between absorbance and incident photon energy ( $h\nu$ ). The TauC plot was used to find the direct band gap for the NPs that is 3.3 eV. The smaller band leads to increased photo degradation behaviour, as electrons are more quickly excited from the valence to conduction band and leads to degradation of dye [22]. The presence of MgO-NPs in the reaction media, which are formed by reducing  $Mg(NO_3)_2$ , is indicated by the sharp peak at 280 nm. Our findings are consistent with previous research [23]. Band gap is influenced by grain size, lattice structure and surface physique [24].

## 2.3. Powder X-Ray Diffraction

The crystalline structure of the particles was verified using X-ray diffraction. Figure 2c shows the XRD patterns of MgO-NPs synthesised by *M. arvensis* leaf extract after total reduction of  $Mg^{2+}$  to  $Mg^0$ . The biosynthesized MgO-NPs showed strong peaks at 2 (degree)  $12.57^\circ$ ,  $20.8^\circ$ ,  $25.68^\circ$ , and  $32.56^\circ$ , which correspond to miller's indices (111), (002), (202), and (113), respectively, conforming to the polycrystalline cubic structure. In XRD patterns, no other impurities were found. The average crystallite size was estimated to be 32.4 nm using the Debye Scherer equation. As mentioned in the process portion, the MgO-NPs were shaped, centrifuged, and redistributed in sterile distilled water prior to XRD examination, removing the existence of any substance that could trigger irregular effects. The appearance of structural peaks in the XRD models explicitly demonstrates that the MgO-NPs synthesised using our green approach are nano-crystalline.

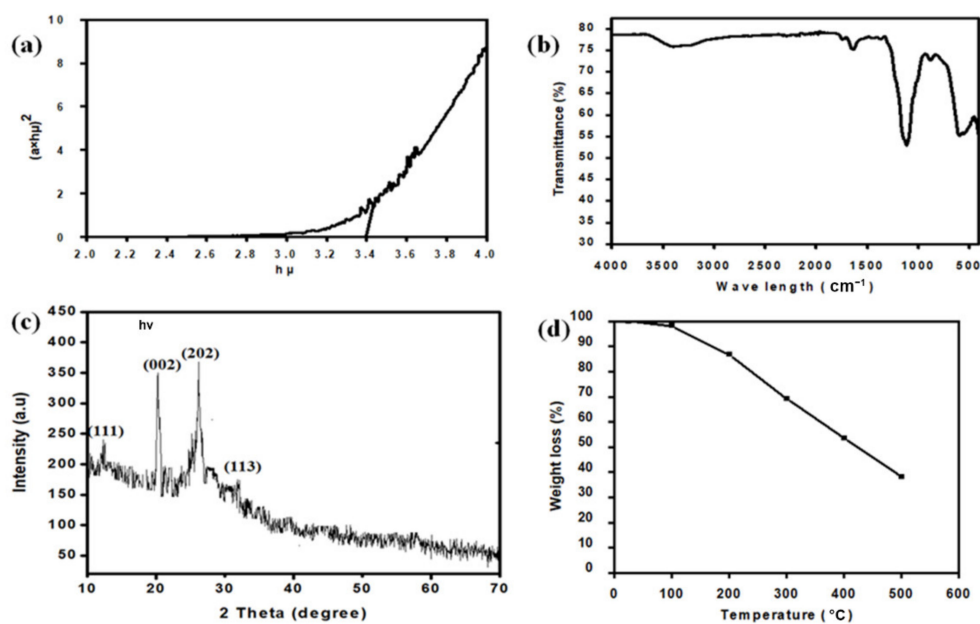


**Figure 2.** (a) Optical Band gap, (b) FTIR spectrum, (c) XRD representation and (d) TGA analysis of Biosynthesized MgO-NPs.

#### 2.4. Fourier Transformed Infrared Spectroscopy

The different functional groups of potential bio molecules present in the plant extract, which serve as synthesised MgO-NPs reduction and capping agents, were identified using FT-IR spectroscopy [25]. Figure 2b shows how FTIR analysis is used to analyse the surface chemistry of biosynthesised NPs. MgO-NPs had notable peaks in their FTIR spectra at  $3461\text{ cm}^{-1}$ ,  $1737\text{ cm}^{-1}$ ,  $1649\text{ cm}^{-1}$ ,  $1151\text{ cm}^{-1}$ ,  $858\text{ cm}^{-1}$ , and  $604\text{ cm}^{-1}$ . The O-H stretching vibration in hydroxyl pairs, C=O stretching vibrations, and C–O–C stretching vibrations are responsible for the absorption peaks at  $3461\text{ cm}^{-1}$ ,  $1737\text{ cm}^{-1}$ , and  $1649\text{ cm}^{-1}$  [26,27]. Peaks at  $1148\text{ cm}^{-1}$  corresponded to O-H folding and C-O stretching of main alcohol functional groups. The broad absorption peak on  $607\text{ cm}^{-1}$  clearly indicated Mg-O bond stretching, indicating that MgO-NPs were successfully synthesized [28]. The FTIR spectra, which also parallels previous studies [25–27], supports the active capping of plant metabolites on the surface of MgO-NPs.

#### 2.5. Thermo Galvanometric Analysis

TGA is a thermal analysis tool that measures changes in material physical and chemical properties as a result of increasing temperature with constant heating. It's used to figure out the properties of materials loss or gain mass due to decomposition, oxidation, or the loss of volatiles [29]. TGA analysis was carried out in the temperature range of  $25\text{ }^{\circ}\text{C}$  to  $600\text{ }^{\circ}\text{C}$ , as seen in Figure 2d. MgO-NPs lost a total of 61.9 percent of their weight. Dehydration and lack of moisture content from the samples was due to the original weight loss up to  $150\text{ }^{\circ}\text{C}$  [30]. Nanoparticles having more plant molecules are susceptible to more weight loss with the increase of temperature. This is due to the breaking of bonds between plant molecules and magnesium ions.

#### 2.6. SEM, TEM and EDX Analysis of MgO-NPs

SEM was used to investigate the size, distribution, and morphology of MgO-NPs, as seen in Figure 3a. The majority of the particles are spherical and can be classified as nanoparticles with an overall size of  $29.72\text{--}40\text{ nm}$  and varying levels of aggregation [25]. The dosage, temperature, and pH of extracts, on the other hand, affect parameters such as nanoparticle size, shape, and agglomeration. Figure 3b shows TEM micrographs of synthesised NPs with circular or elliptical morphology and a mean size of  $29.72\text{--}36\text{ nm}$ .

Using Image J programme, the measurements of about 50 particles were determined for each sample. Similar morphologies have previously been found in the literature [31]. The biomolecules capped the plant sample because the shapes of the particles were brighter than the centres. The MgO-NPs are spherical, as seen by scanning electron micrography, and this is due to interactions and Vander Waals forces. These results are agree with those of previous studies [32]. Figure 3c EDX shows that the MgO-NPs had a high percentage of magnesium as well as a high percentage of oxygen, indicating that MgO-NPs were formed. The extra peaks indicates the elements present in biomolecules of plant [33].

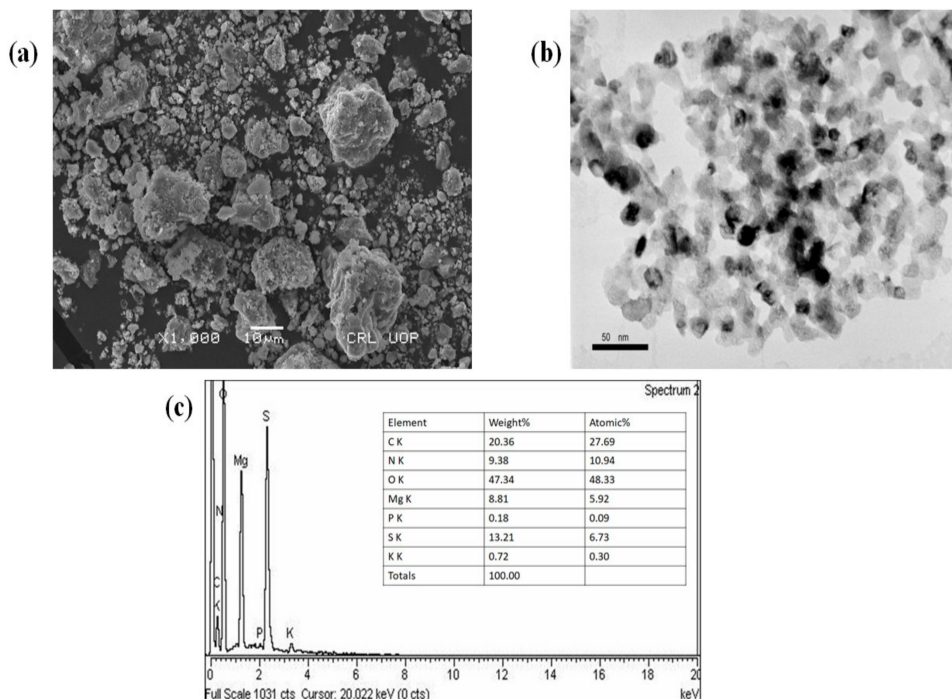


**Figure 3.** (a) SEM micrograph, (b) TEM micrograph and (c) EDX analysis of MgO-NPs.

### 2.7. Zeta Size and Zeta Potential of MgO-NPs

The DLS technique is used to investigate the size distribution and zeta potential ( $\zeta$ ) of biosynthesized MgO-NPs. The zeta potential ( $\zeta$ ) is a common calculation of a particle's surface charge which determines colloidal stability. Stable colloids are described as suspensions with a voltage of 15 mV [34]. The zeta potential of MgO-NPs in distilled water was found to be  $-16.1$  mV in the sample, indicating that the colloidal solution is stable. The dispersion power of the greenly synthesized MgO-NPs is thus checked and supported by the zeta potential measurements. Biomolecules in plant extract and there possible coating and capping during synthesis of nanoparticles leads to negative surface charge [35]. The Zeta hydrodynamic size were  $30$  to  $120 \pm 2$  nm observed via DLS as shown in Figure 4. There were found polydispersity index of  $0.56 \pm 0.04$  in particle size in the size distribution graph obtained via DLS. The tendency of the technique against the estimation of larger particles (or even aggregates) explains the increased scale of the MgO-NPs determined by DLS [34]. The zeta potential of NPs may be affected by distinct functional groups present in plant extract that adsorbed on their surface. Same were also observed by [36].

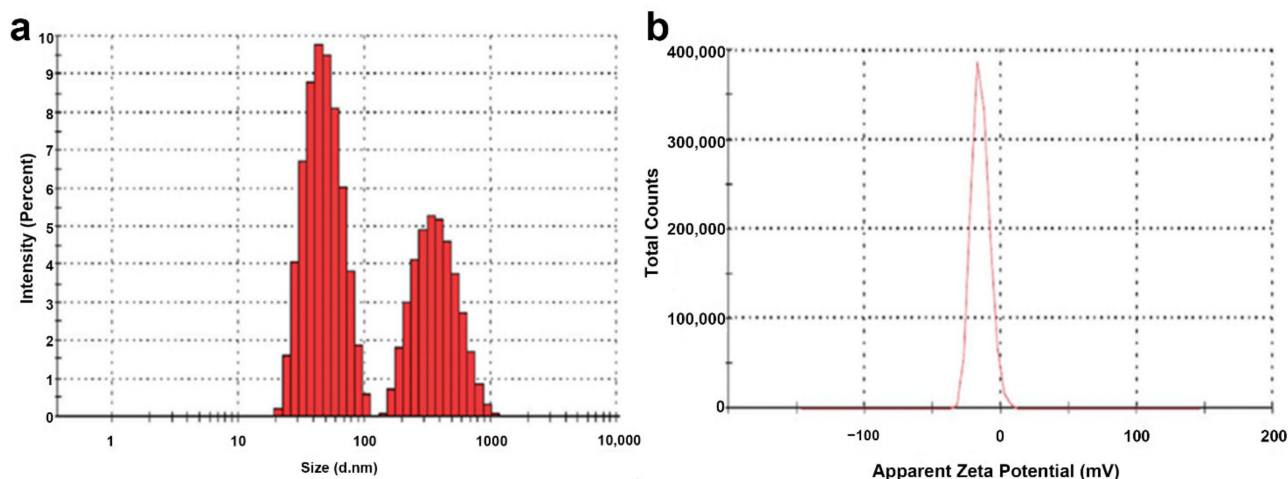


**Figure 4.** (a) Zeta size measurement and (b) Zeta potential measurement of MgO-NPs.

### 2.8. Antibacterial Assay against *H. pylori* Bacterial Isolates

Antimicrobial resistance challenging the world health care system and multidrug-resistant diseases have had a major impact on current antibacterial therapy. Plant-mediated nanomaterials, have a wide therapeutic applications and thus proved itself a new source of antimicrobials [37–39]. In the current situation, environmentally friendly approaches for producing nanomaterials have been a significant technology. Plant mediated nanomaterials gain popularity due to dual function of capping and reduction [40]. In the current research, we synthesised MgO-NPs from a traditional medicinal plant and measured their antibacterial effectiveness against *H. pylori* bacterial strains [41]. The antimicrobial potential of MgO-NPs against test species were shown in Table 1. The study found that various doses of NPs had varying degrees of antimicrobial activity against all microorganisms studied (5 mg/mL, 4 mg/mL, 2 mg/mL and 1 mg/mL). MgO-NPs solution (5 mg/mL) showed the greatest zone of inhibition against *Helicobacter felis* ( $17.19 \pm 0.83$  mm), followed by *Helicobacter suis* ( $16.49 \pm 0.64$  mm) and *Helicobacter salomonis* ( $16.09 \pm 0.66$  mm) in the present report. Our findings are consistent with previous research evaluating the killing ability of MgO-NPs and other metallic NPs against urinary tract infections and *H. pylori* bacterial isolates [42,43].

**Table 1.** Antibacterial potential of MgO-NPs against *H. pylori* isolates.

<i>H. pylori</i> Strains	MgO-NPs			
	5 mg/mL	4 mg/mL	2 mg/mL	1 mg/mL
<i>Helicobacter felis</i>	$17.19 \pm 0.83$ *	$13.32 \pm 0.53$ *	$9.55 \pm 0.56$ *	$6.23 \pm 0.31$ *
<i>Helicobacter suis</i>	$16.49 \pm 0.64$ **	$13.62 \pm 0.51$ *	$9.29 \pm 0.53$ *	$5.48 \pm 0.37$ **
<i>Helicobacter salomonis</i>	$16.09 \pm 0.66$ **	$9.92 \pm 0.42$ ***	$7.70 \pm 0.49$ ***	$5.71 \pm 0.23$ **
<i>Helicobacter bizzozeronii</i>	$14.19 \pm 0.51$ **	$10.23 \pm 0.59$ **	$8.43 \pm 0.41$ **	$4.79 \pm 0.26$ ***
Positive control (Kanamycin)	$21.82 \pm 0.74$	$16.71 \pm 0.82$	$12.67 \pm 0.58$	$12.14 \pm 0.44$

Star \*\*\* represent; \* highly significant, \*\* slightly significant and \*\*\* non-significant difference from control at  $p < 0.05$  by one-way ANOVA in the column Values are mean  $\pm$  SD of triplicate.

### 2.9. Protein Kinase Inhibition Assay

Protein kinase inhibitors are a well-established class of clinically effective medications that has a major role in the treatment of cancer. Since achieving inhibitor selectivity remains a major challenge for researchers, synthesising alternative compounds for chemical biology study or new small molecules as drugs remains a viable option [44,45]. These

enzymes phosphorylate serine-threonine and tyrosine amino acid residues, which play important roles in cell replication, differentiation, and apoptosis. Protein kinase deregulation can contribute to tumor development, so institutions that can suppress these enzymes are crucial in anticancer research [46]. The protein kinase inhibition ability of *M. arvensis* synthesised NPs was tested using the Streptomyces 85E strain. Figure 5a depicts the results. At 0.5 mg/mL, MgO-NPs solution (5 mg/mL) showed the highest zone of inhibition ( $12.44 \pm 0.72$ ) and ( $5.66 \pm 0.44$ ), respectively. Streptomyces strain was inhibited by MgO-NPs in a concentration-dependent manner (Figure 5a). Overall, the findings revealed that all research samples accumulate essential metabolites with anti-cancer properties in *M. arvensis*. The findings are backed up by a previous study that looked at hyphae formation inhibition in Streptomyces 85E and found that isolated compounds displayed a remarkable zone of inhibition at 80 g/disk, leading to the hypothesis that the compounds prevent the formation of hyphae in Streptomyces 85E, which may inhibit cancer proliferation [45,47].

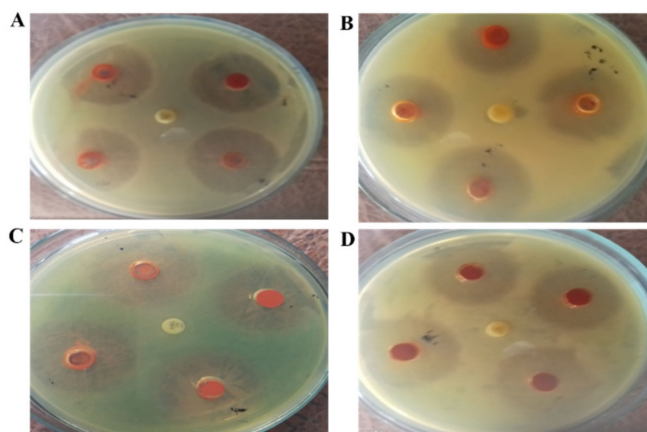


**Figure 5.** Assay picture of NPs against various strains (A) *Helicobacter felis*, (B) *Helicobacter suis*, (C) *Helicobacter salomonis* and (D) *Helicobacter bizzozeronii*.

#### 2.10. In Vitro AChE and BChE Inhibition Assays

Alzheimer's is a neurodegenerative disease and worldwide accounts for sixty to 80 percent cases of dementia. This disease occurrence is alarming, with one person developing Alzheimer's disease every 65 s in the United States alone [48]. Cholinesterase inhibitors are currently available for patients at any stage of Alzheimer's disease. The successful inhibition of cholinesterase enzymes has been identified using a variety of synthetic and natural substances. Hydrolysis of acetyl choline to choline and acetic acid in synapsis in tissues and neuromuscular junctions is catalyzed by these enzymes. Reduced acetyl choline levels contribute to the development of Alzheimer's disease. acetylcholinesterase (AChE) and butrylcholinesterase (BChE) inhibition was investigated using different concentrations of plant extracts [49]. The inhibition of esterases by MgO-NPs was dosage dependent. MgO-NPs were most potent at 400  $\mu\text{g}/\text{mL}$ , inhibiting AChE by  $73.82 \pm 2.19$  percent and BChE by  $69.50 \pm 1.82$  percent. At 25  $\mu\text{g}/\text{mL}$ , AChE had a  $19.63 \pm 0.47\%$  inhibition response and BChE had a  $23.53 \pm 0.51\%$  inhibition response. Overall, as seen by the values in Figure 5b, NPs is found to be highly active against both enzymes. Our findings are consistent with previous research [50,51].

#### 2.11. In Vitro Cytotoxic Potential Against Hela Cell Lines

Only a few studies assessed the apoptotic potential of biosynthesized NPs. The effect of MgO-NPs on HeLa cell proliferation was determined using the MTT assay [52]. This is the first research to test the cytotoxicity of MgO-NPs extracted from *M. arvensis* HeLa cells. The cytotoxic effect against HeLa cells are due to biosynthesized NPs. At the applied concentration, cell death was estimated to be  $49.49 \pm 1.18$  at 400  $\mu\text{g}/\text{mL}$ .

Figures 6c and 7a. Doxorubicin was used as a supportive regulation which resulted in cell death of  $97.11 \pm 3.97$  percent. Sriram et al. [53] and Safaepour et al. [54] addressed a similar cytotoxicity analysis. Metallic NPs are toxic to mammalian cells, according to several in vitro tests. Metallic NPs have been shown in some experiments to have the ability to interfere with genes involved in cell cycle development, as well as cause damage to nucleotides of DNA also induce programmed cell death of ancerous cells. Our findings are in correspondence with [55].

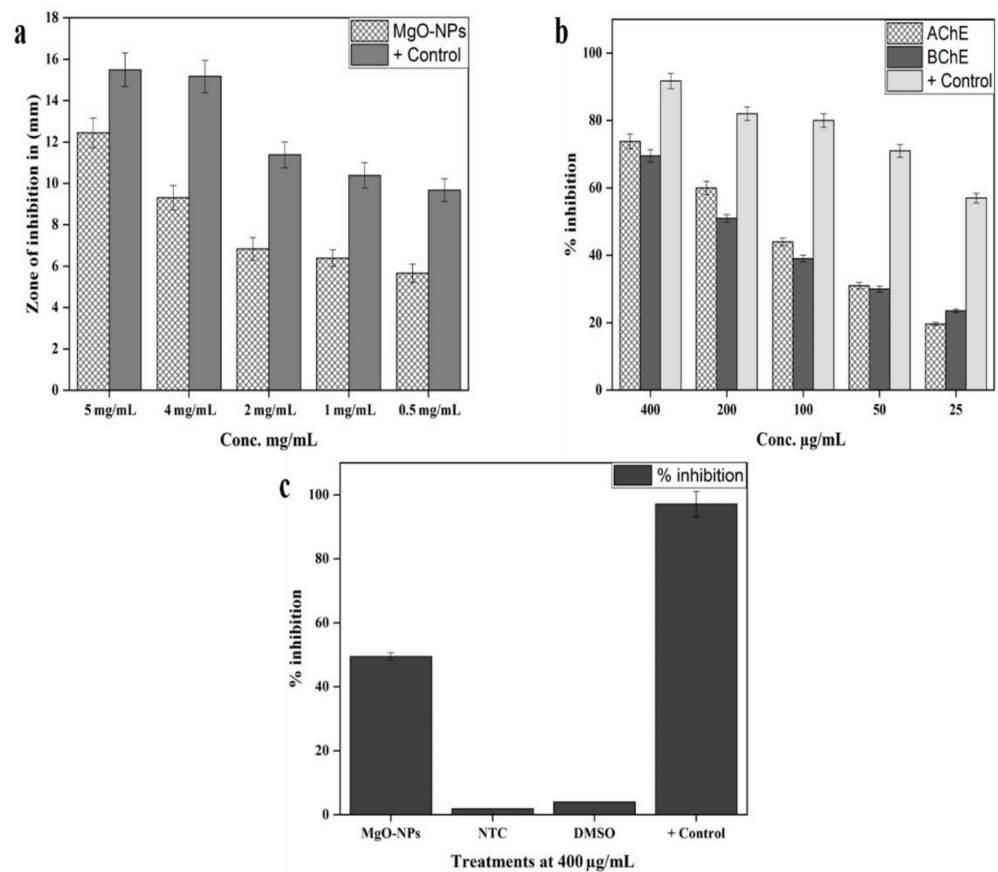


**Figure 6.** (a) Protein kinase inhibition, (b) in vitro AChE and BChE inhibition, (c) Anti-cancer potential of MgO-NPs against Hela Cell Lines.

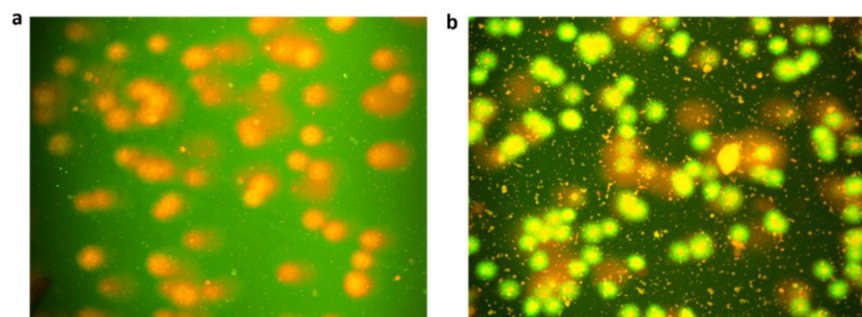


**Figure 7.** (a) Doxorubicin as positive control, (b) MgO-NPs against cell lines.

### 2.12. In Vitro Antioxidant Potential of MgO-NPs

Reactive oxygen species is responsible for the degradation of membrane lipids in cell membrane of plant, degradation of nucleic acids and aminoacids, which results in a shift in plant metabolic pathways [56]. Oxidative stress reaction and plant biomolecules results

in capping and reduction of nanoparticles [57,58]. Total reduction potential, DPPH free radical scavenging, ABTS, and Total antioxidant capability of biosynthesized NPs were assessed. In Table 2, we summarise the antioxidant potential of biosynthesised nanoparticle. Phosphomolbdenum were used to investigate the antioxidant potential of synthesized NPs. The principle of this approach is the reduction of Mo (VI) to Mo (V) in the presence of antioxidant agent, the reduction of Mo form green phosphate molybdenum [59]. The antioxidant potential of biogenic MgO-NPs was at  $61.1 \pm 0.73$  gAAE/mg at  $400 \mu\text{g/mL}$ . With the total reducing power estimate (TRP) assay, total antioxidant potential (TAC) was amplified. The  $\text{Fe}^{3+}$  ion would be converted to  $\text{Fe}^{2+}$  ion if the measured sample has redox potential [60]. The largest TRP, like TAC, was  $43.41 \pm 0.23$  at the highest concentration. ABTS and DPPH free radical scavenging assays were also performed to confirm the TAC and TRP results. The formation of the yellowish diphenyl picrylhydrazine molecule reduces DPPH, which is a stable free radical that is reduced by taking hydrogen or electron from a donor [61]. The antioxidant potential of the sample was confirmed by the quenching of DPPH and ABTS free radicals. MgO-NPs showed maximum scavenging of the DPPH and ABTS free radical at  $400 \mu\text{g/mL}$ , which is  $56.3 \pm 0.38$  and  $77.12 \pm 0.18$  TEAC, respectively. All the assays repeated three times and the average were taken as final reading. Same results were also observed by [41,62].

**Table 2.** Antioxidants potentialities of biosynthesized MgO-NPs.

Conc. ( $\mu\text{g/mL}$ )	TAC ( $\mu\text{g AAE/mg}$ )	TRP ( $\mu\text{g AAE/mg}$ )	ABTS (TEAC)	DPPH (%FRSA)
400	$61.1 \pm 0.73$	$43.41 \pm 0.23$	$77.12 \pm 0.18$	$56.3 \pm 0.38$
200	$55.37 \pm 0.17$	$39.51 \pm 0.47$	$63.63 \pm 0.29$	$41.1 \pm 0.61$
100	$33.86 \pm 0.62$	$22.23 \pm 0.16$	$44.64 \pm 0.46$	$27.69 \pm 0.42$
50	$25.29 \pm 0.56$	$16.76 \pm 0.28$	$25.47 \pm 0.16$	$18.45 \pm 0.88$
25	$19.16 \pm 0.15$	$10.41 \pm 0.86$	$16.39 \pm 0.25$	$10.19 \pm 0.38$

### 2.13. Bio-Compatible Nature of MgO-NPs against Human (RBCs)

Human red blood cells were used in a biocompatibility experiment to demonstrate the biocompatibility of the green synthesised NPs. The haemolysis of erythrocytes against varying Conc. Of NPs ( $25 \mu\text{g/mL}$  to  $400 \mu\text{g/mL}$ ) is observed in this bioassay. A spectrophotometer is used to calculate RBCs haemolysis at 405 nm. Only if the sample has the potential to burst the cell will the RBCs hemolysis be detected. Table 3 shows the biocompatibility effects of our research. The American Society for testing materials has released several recommendations for biocompatibility of compounds, according to which substances with  $>2\%$  haemolysis are called non-haemolytic,  $2\text{--}5\%$  mildly haemolytic, and  $>5\%$  haemolysis are considered haemolytic [63]. As can be seen in Table 3, there are a number of factors to consider. Also at high concentrations, all of our stock solutions of synthesised nanoparticles exhibit fewer haemolysis, demonstrating their high biocompatibility. Also at high concentrations of  $400 \mu\text{g/mL}$ , our biogenic MgO-NPs are hem compatible, and no haemolytic activity is observed at this concentration. As a result of our study's biocompatibility findings, we should conclude that mediated NPs are biosafe and that MgO-NPs can be used as a therapeutic agent.

**Table 3.** % Hemolysis of green synthesized MgO-NPs.

S. No	Conc. $\mu\text{g/mL}$	% Hemolysis
1	400	$2.11 \pm 0.13$
2	200	$2.06 \pm 0.11$
3	100	$1.19 \pm 0.09$
4	50	$0.83 \pm 0.05$

### 3. Discussion

Generally magnesium nanoparticles are synthesized by chemical and physical methods such as chemical vapor deposition, thermal evaporation, sol-gel, sonichemical and spray pyrolysis among others [64]. However, such procedures are high energy demanding, expensive, time consuming and are not eco-friendly [65]. Moreover, chemical methods may result in adsorption of toxic chemicals on the surface of nanoparticles that may lead to adverse effects in biomedical applications [66]. Biological methods that exploit living organism (microbes, plants) or living systems (enzymes) for the synthesis of nanoparticles is one possible alternative for eco-friendly and inexpensive synthesis of MgO-NPs. In the current study, an aqueous extract of *Mentha arvensis* was utilized as reducing and stabilizing agent for the synthesis of multifunctional silver nanoparticles (Ag-NPs). To the best of our knowledge it is the first ever study on *Mentha arvensis* mediated synthesis of magnesium nanoparticles. The main active compounds of *M. arvensis* extracts such as hesperidin, ferulic acid, rosmarinic acid, diosmin, didymin, buddleoside, acacetin and linarin, and have documented numerous biological effects [67].

The species are rich in medicinally important biochemicals including proteins and carbohydrates that played a major role in biosynthesis of MgO-NPs. The initial formation MgO-NPs was indicated by the color change and later on by UV- visible spectroscopy. The band gap of MgO-NPs were calculated as (3.3 eV) respectively, affirming successful synthesis of MgO-NPs [68]. After synthesis, stable MgO-NPs were well characterized by UV- visible spectroscopy, X-ray diffraction (XRD), Fourier transform infrared spectroscopy (FTIR), Dynamic Light Scattering (DLS), Scanning electron microscopy (SEM), Transmission electron microscopy (TEM) and Thermo gravimetric analysis (TGA). Moreover, aqueous dispersion stability of the nanoparticles with varied pH and polarity was also probed as function of storage time. Fourier transformed infrared spectroscopy revealed major functional groups on the synthesized nanoparticles. Major absorption peaks in the FTIR spectra were observed at  $3461\text{ cm}^{-1}$ ,  $1737\text{ cm}^{-1}$ ,  $1649\text{ cm}^{-1}$ ,  $1151\text{ cm}^{-1}$ ,  $858\text{ cm}^{-1}$  and  $604\text{ cm}^{-1}$ . The peaks at  $1148\text{ cm}^{-1}$  corresponded to O-H bending and C-O stretching of the functional groups in primary alcohols. While the broad absorption peak on  $607\text{ cm}^{-1}$  clearly indicated Mg-O bond stretching affirming the successful synthesis of MgO-NPs [28]. The FTIR spectra, thus confirms the successful capping of plant metabolites on the surface of MgO-NPs also resembles with previous reports [69].

X-ray diffraction analysis confirmed high purity of MgO-NPs with no extra peaks and indicated a face centered cubic (FCC) structure of biosynthesized MgO-NPs affirming the highly crystalline nature of the particles. Similar XRD patterns were also reported in previous studies. Moreover, the mean crystallite size as calculated using Scherer equation was found to be 32.4 nm. Furthermore, Thermal gravimetric analysis (TGA) shown that total weight loss of MgO-NPs resulted to be 61.9%. The initial weight loss up to  $150\text{ }^{\circ}\text{C}$  is attributed to the dehydration and loss of moisture content from the samples [70].

Morphology, particle size and elemental composition of MgO-NPs were determined using SEM, TEM and EDX, respectively. SEM micrograph revealed spherical shaped morphology with little degree of aggregation. Similar morphological attributes were also observed in previous reports [71]. Moreover, average particle size of the particles as calculated using ImageJ software from TEM micrographs was found to be  $29.72 \pm 11.36$ . Furthermore, a strong peak at 3 KeV in EDX spectrograph confirmed purity NPs and augment the XRD results.

Dispersion stability plays a vital role in determining functional activities of the engineered nanoparticles in any biological system [72]. Several parameters affect the dispersion capacity of the nanoparticles such as presence of charged or uncharged molecules that are adsorbed on the particle surface and the ionic strength (pH) of the solvent [73]. Our study shown that MgO-NPs form highly stable dispersion in  $\text{H}_2\text{O}$  even after 24 h of sonication. Dynamic Light Scattering studies confirmed the stable Zeta potential ( $\zeta$ ) of  $-16.1\text{ mV}$ . Zeta potential ( $\zeta$ ) defines the colloidal stability and is a typical measurement of the surface charge on the particles. Suspensions that exhibits  $|\zeta| \geq 15\text{ mV}$  are generalized as stable

colloids [73]. The Zeta potential measurement thus verifies and augments to the dispersion capacity of green synthesized MgO-NPs. The  $-ve$  surface charge is due to the binding affinity of the extract compounds on NPs conferring MgO nanoparticles stability and alleviates aggregation potential of the particles [35]. The size distribution graph shows that the particle size is polydispersed and is larger as compared to the TEM observations. The increased size of MgO-NPs measured via DLS is due to the biasness of the technique towards measurement of larger particles (even aggregates) [73]. After physicochemical and morphological characterization the biosynthesized nanoparticles were investigated for multifaceted invitro biomedical applications including Anti *H. pylori*, protein kinase inhibition, anti-Alzheimer's, antioxidant and anticancer potential and biocompatibility against isolated human red blood cells (hRBCs).

Pathogenic microbes cause wide range of diseases in both humans and animals. Novel approaches and sophisticated scientific research has become inevitable for the establishing novel therapeutic strategies to overcome antimicrobial resistance (AMR) and unsystemic use of antibiotics. In general, all the tested bacterial strains showed dose dependent sensitivity against MgO-NPs. Among the bacterial strains, *Helicobacter felis*, and *Helicobacter suis* exhibited high susceptible, displaying considerable zone of inhibition (ZOI) i.e.,  $17.19 \pm 0.83$  mm and  $16.49 \pm 0.64$  mm, respectively. Factors such as size, shape, oxidation state and surface chemistry are considered as the most influential factors dictating antibacterial properties of MgO-NPs. In general recently metal oxide nanoparticles such as zinc, silver, titanium and magnesium based treatments have gained much attention owing to their significant cytotoxicity against *H. pylori* [74]. Ag-NPs has the potential to be used for targeted delivery of potential candidate drugs for Alzheimer's disease. We found interestingly, the inhibition response for both esterases was dose dependent. MgO-NPs were most active at 400  $\mu\text{g}/\text{mL}$  resulted in  $73.82 \pm 2.19\%$  inhibition of AChE and  $69.50 \pm 1.82\%$  for BChE. Our findings, are in agreement with some of the previous studies reported [74]. For preliminary screening for anticancer activity, the biosynthesis nanoparticles were investigated for growth inhibition potential against Protein Kinase. It was observed that MgO-NPs solution (5 mg/mL) displayed maximum zone of inhibition ( $12.44 \pm 0.72$ ) and ( $5.66 \pm 0.44$ ) at 0.5 mg/mL respectively. Due to excellent inhibition activity against Protein Kinase enzyme the particles were further exploited against HeLa cells to verify and augment the anticancer potential.

In our study, MgO-NPs showed potential inhibition of  $49.49 \pm 1.18$  at 400  $\mu\text{g}/\text{mL}$  towards fresh HeLa cells line. There is dearth of data regarding detailed anti-cancerous mechanism of MgO-NPs however certain studies suggest that Ag-NPs results in DNA damage, lysosomal damage, mitochondrial chain and complex disruption and pro apoptotic activity that in turn effect proliferative system and cell cycle of cancer cells ultimately lead to complete inhibition of proliferation. Moreover, the ROS production and associated damages resulting from oxidative stress are highly size dependent with smaller size of MgO-NPs leads to enhanced overproduction of ROS. Smaller particles of MgO-NPs have the capability of increased interaction with cellular compartments and enhanced penetration to release Mg<sup>+</sup> ions [75]. Our findings thus augment and support previously reported studies. Our study thus suggest that biosynthesized Ag-NPs could be used as novel therapeutic agent against HeLa cells. However, detailed in vivo study can be designed to augment the in vitro results and to investigate the detail mechanism involved in anti-cancerous effects.

Furthermore, the biosynthesized nanoparticles were also investigated for antioxidant potential via DPPH (2,2-diphenyl-1-picrylhydrazyl) and ABTS (2,2'-azino-bis(3-ethylbenzothiazoline-6- sulfonic acid) free radical scavenging activity (FRSA), total antioxidant activity (TAC) and total reducing power (TRP) at various concentrations. The particles exhibited dose dependent antioxidant capacity and displayed  $61.1 \pm 0.73$   $\mu\text{gAAE}/\text{mg}$  and  $43.41 \pm 0.23$   $\mu\text{gAAE}/\text{mg}$  TAC and TRP activity at the highest concentration of 400  $\mu\text{g}/\text{mL}$ . While moderate DPPH and ABTS free radical scavenging activity (FRSA) of  $56.3 \pm 0.38$  (IC<sub>50</sub>; 358  $\mu\text{g}/\text{mL}$ ) and  $77.12 \pm 0.18$  TEAC, respectively was noted. From the results

summarized, it can be suggested that some of the antioxidant compounds may be involved in the reduction and stabilization of the NPs during synthesis process and may be responsible for imparting overall moderate antioxidant potential to MgO-NPs. The biocompatibility of the engineered nanomaterial (ENMs) is an essential requirement for biomedical applications. The particles exhibited excellent hemocompatibility as even at the highest concentration of 400 µg/mL 2.11 ± 0.13 haemolysis activity was observed. Our finding thus, endorses the bio safe nature of the particles and thus pave the way for *Mentha arvensis* synthesized MgO-NPs be subjected for therapeutic applications.

#### 4. Materials and Methods

##### 4.1. Collection and Processing of the Plant Material

The herb used in this analysis was collected in the district of Charsadda in the Pakistani province of Khyber Pakhtunkhwa. The plant was confirmed as *Mentha arvensis* by the professors in Department of Botany, Bacha Khan University in Charsadda, Pakistan. Leaves were taken from the plant and dried in shade followed by grinding in to powder form and stored at 25 °C for extraction process. 30 g of plant powder were mixed with 200 mL of deionized water and properly shaken for 10 min, followed by incubation at 200 rpm in sun scientific orbital shaking incubator model number ES 20. The obtain extract was filtered thrice with nylon cloth and thrice with Whatman filter paper to remove any remaining residues. The extract were stored for future use in the experiment.

##### 4.2. Biosynthesis of MgO Nanoparticles

With minor modifications, MgO-NPs were synthesised according to a published protocol [12]. In a nutshell, 100 mL plant extract was mixed with 6.0 g of Mg(NO<sub>3</sub>)<sub>2</sub>·6H<sub>2</sub>O and leftover at 60 °C for 2 h on a magnetic stirrer. The mixture were centrifuged at 1000 rpm just after the completion of the reaction. The pellets were washed three times with distilled water and then kept in oven to be dried and after that the particles were calcinated for 2 h at 500 °C. The nanoparticles were grinded in to fine powder and stored in a vial for physiochemical characterization.

##### 4.3. Characterizations of Biosynthesized MgO-NPs

Physicochemical properties of *M. arvensis* synthesised MgO-NPs were investigated using various characterization techniques. 200 to 700 nm standard wavelenth was used in UV analysis of MgO-NPs [76]. The X-ray diffraction method was used to detect the crystallite nature of green synthesised MgO-NPs. XRD spectra were obtained by PANalyticaX'pert diffractometer (Company, City, State abbr, Country). The Scherer's standard equation were evaluated to determine the crystal size [77].

$$D = k \lambda / \beta \cos\theta$$

D represents half-peak-height of an XRD line due to a specific crystalline plane K denotes shape factor (0.94), λ depicts X-rays wavelength of 1.5421 Å while β and θ refers to FWHM in radians and Bragg's angle, respectively". Fourier transforming infrared spectroscopic analysis were performed in 400 cm<sup>-1</sup> to 4000 cm<sup>-1</sup> spectral range to detect the functional group responsible for nanoparticle formulation by using Jasco FT/IR-6000 FTIR spectrometer [78]. SEM (JSM-7600F, Japan) and TEM (JEM-2100F, Japan) were used to analyse morphology and physical measurements, while EDX with TEM (JEM2100) INCA100/Oxford instruments, U.K. were used to know about the elemental composition of MgO-NPs [79]. The electrostatic Zeta potential arises at a particle's shear plane and affects all surface charges and the particle's local medium. The Zeta Potential Analyzer is used to examine the Zeta potential. For logging all of the measurements, phase analysis Light Scattering Mastersizer 3000 were used calculate Zeta Potential were calculated via Smoluchowski equation.

$$V = (\epsilon E / \eta) \zeta$$

where  $v$  = electrophoretic velocity,  $\eta$  = viscosity,  $\epsilon$  = electrical permittivity of the electrolytic solution and  $E$  = electric field [80]. Thermo Gravimetric Analysis was used to investigate thermal equilibrium using a Q500 thermo gravimetric analyser Pyris Diamond Series TG/DTA under flowing nitrogen gas at a. at a temperature of 30 °C to 600 °C.

#### 4.4. Antibacterial Assay of MgO-NPs against *H. pylori* Bacterial Strains

The antibacterial activity of test samples was assessed using the agar well diffusion process, as previously described [81]. *Helicobacter bizzozeronii*, *Helicobacter felis*, *Helicobacter salomonis*, and *Helicobacter suis* were among the bacteria included in the report. Using the MacFarland specifications. Following that, 50 L of fresh culture is spilled onto nutrient agar plates and evenly scattered with cotton swabs. 5 mm wells were made with a sterile borer, and 10 L of the examined samples were applied, with the plates labelled accordingly. The concentrations ranged from 1 mg/mL to 5 mg/mL. Kanamycin and DMSO were used as positive and negative controls, respectively, in the assay. After that, the bacterial culture plates were incubated at 37 °C for overnight. Zones of inhibition were measured by using Vernier Calliper.

#### 4.5. Protein Kinase Inhibition Assay

This assay is used to test the anticancer function of biosynthesized MgO-NPs. This is a bioassay for confirming the synthesised NPs' capacity to suppress protein kinases [47]. Adopted a protocol that was subtly different from ours. *Streptomyces* 85E was used as a research strain. 100 mL of *Streptomyces* 85E culture were poured into ISP4 medium plates. Each well (5 mm) was filled with around 5 L of MgO-NPs and labelled accordingly. Surfactin was used as a +ve, while DMSO as a –ve control. After that plates were incubated for two days at 28 degrees Celsius. Clear and bald areas around wells were observed, which indicate that phosphorylation, mycelia, and spore formation have been inhibited. The cytotoxic potential of MgO-NPs were observed by strong inhibition zones.

#### 4.6. Anti-Alzheimer's Activity

Inhibition of the enzymes Acetylcholinesterase (AChE) and Butyrylcholinesterase (BChE) may be a target in Alzheimer's treatment. The inhibition power of MgO-NPs by AChE (Sigma "101292679") (St. Louis, MI, USA) and BChE (Sigma "101303874") was investigated using Elman's protocol [82], which was slightly modified. The concentration level for the reference sample was 12.5 µg/mL to 400 µg/mL. Phosphate buffer saline (PBS) solution was used to diffuse the NPs. In AChE, the final enzyme concentration was 0.03U/mL, while in BChE, it was 0.01 U/mL. The reaction mixture, which included DTNB (0.00022 M), BTChI (0.0005 M), and ATChI (0.0005 M), was prepared in purified water and stored at 4 °C. The positive control was Methanol-mediated Galanthamine hydrobromide (Sigma; GI660), while the negative control was the reaction combination without the reference sample. The anticholinesterase assay works by hydrolyzing ATChI and BTChI into AChE and BChE, respectively, resulting in the formation of 5-thio-2-nitrobenzoate anion. The latter forms further complexes with DTNB, resulting in a yellow colour. Absorbance was measured using a UV-VIS spectrophotometer set to 412 nm. With a decrease in absorption rate over time, galantamine and MgO-NPs can be used to calculate percent enzyme inhibition and percent enzyme activity.

$$V = \Delta\text{Abs}/\Delta t$$

$$\text{Enzyme activity (\%)} = V/V_{\text{max}} \times 100$$

$$\text{Enzyme inhibition (\%)} = 100 - \text{Enzyme activity (\%)}$$

#### 4.7. Anti-Cancer Potential of MgO-NPs against HeLa Cell Lines

HeLa cells were obtained from the University of Peshawar in Pakistan. HeLa cells were cultured in MEM & McCoys 5a media, the media were supplemented with 10%

calf serum and incubated with 5% CO<sub>2</sub>. HeLa cells were seeded in to 96 well plates 1 × 10<sup>4</sup> cells per plate and incubated for two days at 37 °C. HeLa cells were treated with biosynthesized MgO-NPs and controls at a fix concentration of 400 µg/mL. Simultaneously, HeLa cells were also treated with Doxorubicin (a well-known anticancer agent having Conc. of 100 mM). The paltes were incubated for 2–3 days to examine the cytotoxic potential of MgO-NPs. The MTT assay was then performed on these plates. MTT solution is prepared at a concentration of 5 mg/mL. Every well received 100 mL of MTT, which was incubated for 4 h. Since forming purple-colored formazone crystals, di-methyl sulphoxide was used to dissolve them (DMSO). At 620 nm In ELISA plate reader the samples were observed. The foolowing formula were used to calculate the anticancer potential of NPs.

Percentage of viability = OD value of experimental sample (MgO-NPs)/OD value of experimental control (untreated) × 100.

#### 4.8. Estimation of Antioxidant Activity

##### 4.8.1. DPPH Antioxidant Assay

The antioxidant function of DPPH (2,2-diphenyl-1-picrylhydrazyl) was calculated using the previously published protocol [83] with slight modifications. Sample extract (20 L) was combined with DPPH (3.2 mg/100 mL methanol) 180 L, and the mixture was incubated at 25 °C for 1 h before adding dH<sub>2</sub>O (160 L). The absorbance at 517 nm was measured using an absorbance microplate reader. The methanolic extract and 0.5 mL of DPPH solution were used as standards to map the calibration curve (R<sub>2</sub> = 0.989). The percent radical scavenging potential of MgO-NPs were calculated by following formula.

$$\text{Freeradicalscavengingactivity(\%)} = 100 \times \left( 1 - \frac{Ac}{As} \right)$$

##### 4.8.2. Total Antioxidant Capacity Determination (TAC)

Protocol stated by [84] were used to determine overall antioxidant ability. Using a micropipette, 1 mL of sample was filled into Eppendorf tubing. Then we fill Eppendorf tubes with 0.9 mL of TAC reagent Followed by incubation at 90 °C for 48 h in a water bath. The sample absorbance were measured at 630 nm in microplate reader and total antioxidant capacity of MgO-NPs were calculated in ascorbic acid equivalent/mg units.

##### 4.8.3. Total Reducing Power Determination (TRP)

The same technique as described by [85] were employed to determine TRP. The research sample was still in an Eppendorf tube, so 400 µL of 0.2 M phosphate buffer with pH 6.6 and potassium ferric cyanide (1 percent *w/v*) added to it and followed by incubation at 55 °C for half an hour in water bath and each Eppendorf tube was filled with 400 µL of trichloroacetic acid (10% *w/v*) after incubation which is followed centrifugation at 3000 rpm for 10 min. The supernatant (140 µL) obtained after centrifugation were poured into 96-well plate that already contained 60 µL of ferric cyanide solution (0.1 percent *w/v*). The absorbance of the sample in microplate reader was set to 630 nm for reading.

##### 4.8.4. Antioxidant ABTS Assay

Previous methods [84] were used in this experiment. In a nutshell, the ABTS solution were prepared by combining 7 mM ABTS salt with 2.45 mM potassium persulphate in an equal proportion and storing the mixture in the dark for 16 h. Until combining with extracts, the solvent absorbance was measured at 734 nm and calibrated to 0.7. The mixture was left in the dark for another 15 min at 25 °C. The absorbance was measured at 734 nm.

#### 4.9. Biocompatibility Studies

New human red blood cells (hRBCs) were used to explain biogenic MgO-NPs bio-compatibility [85]. After the individual's consent, 1 mL of blood samples were collected in EDTA tubes from healthy individuals followed by centrifugation to isolate RBCs. Pellets

were rinsed with PBS. Following centrifugation to isolate RBCs. 200 mL of RBCs and PBS (9.8 mL) at pH: 7.2 were gently mixed for preparation of suspension. MgO-NPs were reacted with erythrocyte suspension at different Conc. followed by incubation for 1 h at 35 °C. The reaction mixture were centrifuged and transfer to well plate to detect haemoglobin release at standart absorption peak of 450 nm. The formula for calculating percent haemolysis was:

$$(\%) \text{ Haemolysis} = \left( \frac{\text{sample Ab} - \text{negative control Ab}}{\text{Positive control Ab} - \text{Negative control Ab}} \right) \times 100$$

## 5. Conclusions

This study focuses on an environmental friendly synthesis of MgO-NPs from *Mentha arvensis* XRD spectra confirms the crystalline structure of MgO-NPs. The presence of phytochemicals involved in the transition of ions was confirmed using Fourier transforming infrared spectroscopy (FTIR). SEM and TEM analysis were used to decide morphology and vibrational modes, while DLS was used to determine surface charge and stability, and TGA was used to determine stability. MgO-NPs that have been synthesised have proven to be effective antioxidants and antibacterial strains. Bioengineered MgO-NPs have a high inhibitory potential against AChE and BChE enzymes. Biogenic MgO-NPs were discovered to be highly effective against Hela cell lines. Human red blood cells have been shown to be biocompatible with synthesised MgO-NPs. Our study concluded that the biogenic MgO-NPs described above can be used in a variety of diseases, cosmetics, and cancer studies. More research into the use of magnesium oxide nanoparticles in biomedicine, both in vitro and in vivo, is required.

**Author Contributions:** Conceptualization, S.F.; methodology, S.F.; software, A., M.R., H.J., S.A.S. and S.S.; validation, M.I., N.B. and R.M.; formal analysis, M.R., Z.H., W.K. and A.I.; investigation, M.N.U. and N.Z.; data curation, M.R. and A.K.; A writing—original draft preparation, S.F.; A writing—review and editing, H.J.; visualization, S.S.; supervision, S.A.S. All authors have read and agreed to the published version of the manuscript.

**Funding:** This research received no external funding.

**Data Availability Statement:** All required data is present in this file.

**Acknowledgments:** We are thankful to Institute of Biotechnology and Microbiology, Bacha Khan University Charsadda, KPK, Pakistan. for their support and facilities.

**Conflicts of Interest:** The authors declare no conflict of interest.

## References

1. Ramsden, J. *Nanotechnology: An Introduction*; William Andrew: Norwich, NY, USA, 2016.
2. Albrecht, M.A.; Evans, C.W.; Raston, C.L. Green chemistry and the health implications of nanoparticles. *Green Chem.* **2006**, *8*, 417–432. [[CrossRef](#)]
3. Herlekar, M.; Barve, S.; Kumar, R. Plant-mediated green synthesis of iron nanoparticles. *J. Nanoparticles* **2014**, *2014*. [[CrossRef](#)]
4. Simonis, F.; Schilthuisen, S. *Nanotechnology; Innovation Opportunities for Tomorrow's Defence*, Report; TNO Science & Industry Future Technology Center: Delft, The Netherlands, 2006.
5. Iravani, S. Green synthesis of metal nanoparticles using plants. *Green Chem.* **2011**, *13*, 2638–2650. [[CrossRef](#)]
6. Duan, H.; Wang, D.; Li, Y. Green chemistry for nanoparticle synthesis. *Chem. Soc. Rev.* **2015**, *44*, 5778–5792. [[CrossRef](#)]
7. Bala, N.; Saha, S.; Chakraborty, M.; Maiti, M.; Das, S.; Basu, R.; Nandy, P. Green synthesis of zinc oxide nanoparticles using Hibiscus subdariffa leaf extract: Effect of temperature on synthesis, anti-bacterial activity and anti-diabetic activity. *RSC Adv.* **2015**, *5*, 4993–5003. [[CrossRef](#)]
8. Hasan, S. A review on nanoparticles: Their synthesis and types. *Res. J. Recent Sci.* **2015**, *2277*, 2502.
9. Barzinjy, A.A.; Hamad, S.M.; Aydın, S.; Ahmed, M.H.; Hussain, F.H. Green and eco-friendly synthesis of Nickel oxide nanoparticles and its photocatalytic activity for methyl orange degradation. *J. Mater. Sci. Mater. Electron.* **2020**, *31*, 11303–11316. [[CrossRef](#)]
10. Tang, Z.-X.; Lv, B.-F. MgO nanoparticles as antibacterial agent: Preparation and activity. *Braz. J. Chem. Eng.* **2014**, *31*, 591–601. [[CrossRef](#)]

11. Fernández-García, M.; Rodríguez, J.A. Metal oxide nanoparticles. In *Encyclopedia of Inorganic and Bioinorganic Chemistry*; John Wiley & Sons, Ltd.: Hoboken, NJ, USA, 2011.
12. Vergheese, M.; Vishal, S.K. Green synthesis of magnesium oxide nanoparticles using *Trigonella foenum-graecum* leaf extract and its antibacterial activity. *J. Pharm. Phytochem.* **2018**, *7*, 1193–1200.
13. Bindhu, M.; Umadevi, M.; Micheal, M.K.; Arasu, M.V.; Al-Dhabi, N.A. Structural, morphological and optical properties of MgO nanoparticles for antibacterial applications. *Mater. Lett.* **2016**, *166*, 19–22. [[CrossRef](#)]
14. El-Moslami, S.H. Bioprocessing strategies for cost-effective large-scale biogenic synthesis of nano-MgO from endophytic *Streptomyces coelicolor* strain E72 as an anti-multidrug-resistant pathogens agent. *Sci. Rep.* **2018**, *8*, 1–22. [[CrossRef](#)]
15. Jeevanandam, J.; San Chan, Y.; Danquah, M.K. Biosynthesis and characterization of MgO nanoparticles from plant extracts via induced molecular nucleation. *New J. Chem.* **2017**, *41*, 2800–2814. [[CrossRef](#)]
16. Thawkar, B.S. Phytochemical and pharmacological review of *Mentha arvensis*. *Int. J. Green Pharm. (IJGP)* **2016**, *10*, 2.
17. do Nascimento, E.M.M.; Rodrigues, F.F.G.; Campos, A.R.; da Costa, J.G.M. Phytochemical prospection, toxicity and antimicrobial activity of *Mentha arvensis* (Labiatae) from northeast of Brazil. *J. Young Pharm.* **2009**, *1*, 210.
18. Chan, K. *Mentha Spicata-A Potential Cover Crop for Tropical Conservation Agriculture*; University of Hawaii at Manoa: Honolulu, HI, USA, 2016.
19. Zhao, B.T.; Kim, T.I.; Kim, Y.H.; Kang, J.S.; Min, B.S.; Son, J.K.; Woo, M.H. A comparative study of *Mentha arvensis* L. and *Mentha haplocalyx* Briq. by HPLC. *Nat. Prod. Res.* **2018**, *32*, 239–242. [[CrossRef](#)]
20. Adomako-Bonsu, A.G.; Chan, S.L.; Pratten, M.; Fry, J.R. Antioxidant activity of rosmarinic acid and its principal metabolites in chemical and cellular systems: Importance of physico-chemical characteristics. *Toxicol. In Vitro* **2017**, *40*, 248–255. [[CrossRef](#)]
21. Guilger-Casagrande, M.; de Lima, R. Synthesis of Silver Nanoparticles Mediated by Fungi: A Review. *Front. Bioeng. Biotechnol.* **2019**, *7*. [[CrossRef](#)]
22. Balakrishnan, G.; Velavan, R.; Batoor, K.M.; Raslan, E.H. Microstructure, optical and photocatalytic properties of MgO nanoparticles. *Results Phys.* **2020**, *16*, 103013. [[CrossRef](#)]
23. Bhargava, R.; Khan, S. Superior dielectric properties and bandgap modulation in hydrothermally grown Gr/MgO nanocomposite. *Phys. Lett. A* **2019**, *383*, 1671–1676. [[CrossRef](#)]
24. Wang, F.-H.; Chang, C.-L. Effect of substrate temperature on transparent conducting Al and F co-doped ZnO thin films prepared by rf magnetron sputtering. *Appl. Surf. Sci.* **2016**, *370*, 83–91. [[CrossRef](#)]
25. Sushma, N.J.; Prathyusha, D.; Swathi, G.; Madhavi, T.; Raju, B.D.P.; Mallikarjuna, K.; Kim, H.-S. Facile approach to synthesize magnesium oxide nanoparticles by using *Clitoria ternatea*—Characterization and in vitro antioxidant studies. *Appl. Nanosci.* **2016**, *6*, 437–444. [[CrossRef](#)]
26. Jayaseelan, C.; Ramkumar, R.; Rahuman, A.A.; Perumal, P. Green synthesis of gold nanoparticles using seed aqueous extract of *Abelmoschus esculentus* and its antifungal activity. *Ind. Crops Prod.* **2013**, *45*, 423–429. [[CrossRef](#)]
27. Nguyen, D.T.C.; Dang, H.H.; Vo, D.-V.N.; Bach, L.G.; Nguyen, T.D.; Van Tran, T. Biogenic synthesis of MgO nanoparticles from different extracts (flower, bark, leaf) of *Tecoma stans* (L.) and their utilization in selected organic dyes treatment. *J. Hazard. Mater.* **2021**, *404*, 124146. [[CrossRef](#)]
28. Nandgaonkar, A.G. Bacterial Cellulose (BC) as a Functional Nanocomposite Biomaterial. Ph.D. Thesis, North Carolina State University, Raleigh, NC, USA, 2014.
29. Mašek, O.; Budarin, V.; Gronnow, M.; Crombie, K.; Brownsort, P.; Fitzpatrick, E.; Hurst, P. Microwave and slow pyrolysis biochar—Comparison of physical and functional properties. *J. Anal. Appl. Pyrolysis* **2013**, *100*, 41–48. [[CrossRef](#)]
30. Jhansi, K.; Jayarambabu, N.; Reddy, K.P.; Reddy, N.M.; Suvarna, R.P.; Rao, K.V.; Kumar, V.R.; Rajendar, V. Biosynthesis of MgO nanoparticles using mushroom extract: Effect on peanut (*Arachis hypogaea* L.) seed germination. *3 Biotech* **2017**, *7*, 1–11. [[CrossRef](#)]
31. Suresh, J.; Pradheesh, G.; Alexramani, V.; Sundrarajan, M.; Hong, S.I. Green synthesis and characterization of hexagonal shaped MgO nanoparticles using insulin plant (*Costus pictus* D. Don) leave extract and its antimicrobial as well as anticancer activity. *Adv. Powder Technol.* **2018**, *29*, 1685–1694. [[CrossRef](#)]
32. Rahmani-Nezhad, S.; Dianat, S.; Saeedi, M.; Hadjiakhoondi, A. Synthesis, characterization and catalytic activity of plant-mediated MgO nanoparticles using *Mucuna pruriens* L. seed extract and their biological evaluation. *J. Nanoanal.* **2017**, *4*, 290–298.
33. Wong, C.W.; San Chan, Y.; Jeevanandam, J.; Pal, K.; Bechelany, M.; Abd Elkodous, M.; El-Sayyad, G.S. Response surface methodology optimization of mono-dispersed MgO nanoparticles fabricated by ultrasonic-assisted sol-gel method for outstanding antimicrobial and antibiofilm activities. *J. Clust. Sci.* **2020**, *31*, 367–389. [[CrossRef](#)]
34. Mourdikoudis, S.; Pallares, R.M.; Thanh, N.T. Characterization techniques for nanoparticles: Comparison and complementarity upon studying nanoparticle properties. *Nanoscale* **2018**, *10*, 12871–12934. [[CrossRef](#)]
35. Vimala, K.; Sundarraj, S.; Paulpandi, M.; Vengatesan, S.; Kannan, S. Green synthesized doxorubicin loaded zinc oxide nanoparticles regulates the Bax and Bcl-2 expression in breast and colon carcinoma. *Process Biochem.* **2014**, *49*, 160–172. [[CrossRef](#)]
36. Lynch, I.; Dawson, K.A. Protein-nanoparticle interactions. *Nano Today* **2008**, *3*, 40–47. [[CrossRef](#)]
37. Romero, C.D.; Chopin, S.F.; Buck, G.; Martinez, E.; Garcia, M.; Bixby, L. Antibacterial properties of common herbal remedies of the southwest. *J. Ethnopharmacol.* **2005**, *99*, 253–257. [[CrossRef](#)]
38. Boucher, H.W.; Talbot, G.H.; Bradley, J.S.; Edwards, J.E.; Gilbert, D.; Rice, L.B.; Scheld, M.; Spellberg, B.; Bartlett, J. Bad bugs, no drugs: No ESKAPE! An update from the Infectious Diseases Society of America. *Clin. Infect. Dis.* **2009**, *48*, 1–12. [[CrossRef](#)] [[PubMed](#)]

39. Talbot, G.H.; Bradley, J.; Edwards, J.E., Jr.; Gilbert, D.; Scheld, M.; Bartlett, J.G. Bad bugs need drugs: An update on the development pipeline from the Antimicrobial Availability Task Force of the Infectious Diseases Society of America. *Clin. Infect. Dis.* **2006**, *42*, 657–668. [[CrossRef](#)]
40. Saif, S.; Tahir, A.; Chen, Y. Green synthesis of iron nanoparticles and their environmental applications and implications. *Nanomaterials* **2016**, *6*, 209. [[CrossRef](#)]
41. Rajeshkumar, S.; Menon, S.; Kumar, S.V.; Tambuwala, M.M.; Bakshi, H.A.; Mehta, M.; Satija, S.; Gupta, G.; Chellappan, D.K.; Thangavelu, L. Antibacterial and antioxidant potential of biosynthesized copper nanoparticles mediated through *Cissus amotiana* plant extract. *J. Photochem. Photobiol. B Biol.* **2019**, *197*, 111531. [[CrossRef](#)]
42. Gurunathan, S.; Jeong, J.-K.; Han, J.W.; Zhang, X.-F.; Park, J.H.; Kim, J.-H. Multidimensional effects of biologically synthesized silver nanoparticles in *Helicobacter pylori*, *Helicobacter felis*, and human lung (L132) and lung carcinoma A549 cells. *Nanoscale Res. Lett.* **2015**, *10*, 1–17. [[CrossRef](#)] [[PubMed](#)]
43. Safarov, T.; Kiran, B.; Bagirova, M.; Allahverdiyev, A.M.; Abamor, E.S. An overview of nanotechnology-based treatment approaches against *Helicobacter Pylori*. *Expert Rev. Anti Infect. Ther.* **2019**, *17*, 829–840. [[CrossRef](#)] [[PubMed](#)]
44. Ferguson, F.M.; Gray, N.S. Kinase inhibitors: The road ahead. *Nat. Rev. Drug Discov.* **2018**, *17*, 353. [[CrossRef](#)] [[PubMed](#)]
45. Jan, H.; Shah, M.; Usman, H.; Khan, A.; Muhammad, Z.; Hano, C.; Abbasi, B.H. Biogenic Synthesis and Characterization of Antimicrobial and Anti-parasitic Zinc Oxide (ZnO) Nanoparticles using Aqueous Extracts of the Himalayan Columbine (*Aquilegia pubiflora*). *Front. Mater.* **2020**, *7*, 249. [[CrossRef](#)]
46. Bain, J.; Plater, L.; Elliott, M.; Shpiro, N.; Hastie, C.J.; Mclauchlan, H.; Klevernic, I.; Arthur, J.S.C.; Alessi, D.R.; Cohen, P. The selectivity of protein kinase inhibitors: A further update. *Biochem. J.* **2007**, *408*, 297–315. [[CrossRef](#)] [[PubMed](#)]
47. Jan, H.; Khan, M.A.; Usman, H.; Shah, M.; Ansir, R.; Faisal, S.; Ullah, N.; Rahman, L. The *Aquilegia pubiflora* (*Himalayan columbine*) mediated synthesis of nanoceria for diverse biomedical applications. *RSC Adv.* **2020**, *10*, 19219–19231. [[CrossRef](#)]
48. Weller, J.; Budson, A. Current understanding of Alzheimer’s disease diagnosis and treatment. *F1000Research* **2018**, *7*. [[CrossRef](#)] [[PubMed](#)]
49. Khalil, A.T.; Ayaz, M.; Ovais, M.; Wadood, A.; Ali, M.; Shinwari, Z.K.; Maaza, M. In vitro cholinesterase enzymes inhibitory potential and in silico molecular docking studies of biogenic metal oxides nanoparticles. *Inorg. Nano Met. Chem.* **2018**, *48*, 441–448. [[CrossRef](#)]
50. Hassan, D.; Khalil, A.T.; Saleem, J.; Diallo, A.; Khamlich, S.; Shinwari, Z.K.; Maaza, M. Biosynthesis of pure hematite phase magnetic iron oxide nanoparticles using floral extracts of *Callistemon viminalis* (bottlebrush): Their physical properties and novel biological applications. *Artif. Cells Nanomed. Biotechnol.* **2018**, *46* (Suppl. 1), 693–707. [[CrossRef](#)]
51. Šinko, G.; Vrček, I.V.; Goessler, W.; Leitinger, G.; Dijanošić, A.; Miljanić, S. Alteration of cholinesterase activity as possible mechanism of silver nanoparticle toxicity. *Environ. Sci. Pollut. Res.* **2014**, *21*, 1391–1400. [[CrossRef](#)]
52. Sukirtha, R.; Priyanka, K.M.; Antony, J.J.; Kamalakkannan, S.; Thangam, R.; Gunasekaran, P.; Krishnan, M.; Achiraman, S. Cytotoxic effect of Green synthesized silver nanoparticles using *Melia azedarach* against in vitro HeLa cell lines and lymphoma mice model. *Process Biochem.* **2012**, *47*, 273–279. [[CrossRef](#)]
53. Sriram, M.I.; Kanth, S.B.M.; Kalishwaralal, K.; Gurunathan, S. Antitumor activity of silver nanoparticles in Dalton’s lymphoma ascites tumor model. *Int. J. Nanomed.* **2010**, *5*, 753.
54. Safaepour, M.; Shahverdi, A.R.; Shahverdi, H.R.; Khorramizadeh, M.R.; Gohari, A.R. Green synthesis of small silver nanoparticles using geraniol and its cytotoxicity against fibrosarcoma-wehi 164. *Avicenna J. Med Biotechnol.* **2009**, *1*, 111. [[PubMed](#)]
55. Sanpui, P.; Chattopadhyay, A.; Ghosh, S.S. Induction of apoptosis in cancer cells at low silver nanoparticle concentrations using chitosan nanocarrier. *ACS Appl. Mater. Interfaces* **2011**, *3*, 218–228. [[CrossRef](#)]
56. Sergiev, I.; Todorova, D.; Shopova, E.; Jankauskiene, J.; Jankovska-Bortkevič, E.; Jurkonienė, S. Exogenous auxin type compounds amend PEG-induced physiological responses of pea plants. *Sci. Hortic.* **2019**, *248*, 200–205. [[CrossRef](#)]
57. Mohamed, H.I.; Akladios, S.A. Changes in antioxidants potential, secondary metabolites and plant hormones induced by different fungicides treatment in cotton plants. *Pestic. Biochem. Physiol.* **2017**, *142*, 117–122. [[CrossRef](#)]
58. Rehman, M.; Ullah, S.; Bao, Y.; Wang, B.; Peng, D.; Liu, L. Light-emitting diodes: Whether an efficient source of light for indoor plants? *Environ. Sci. Pollut. Res.* **2017**, *24*, 24743–24752. [[CrossRef](#)]
59. Prieto, M.; Curran, T.P.; Gowen, A.; Vázquez, J.A. An efficient methodology for quantification of synergy and antagonism in single electron transfer antioxidant assays. *Food Res. Int.* **2015**, *67*, 284–298. [[CrossRef](#)]
60. Skonieczna, M.; Hudy, D. Biological activity of Silver Nanoparticles and their applications in Anticancer Therapy. In *Biological Activity of Silver Nanoparticles and Their Applications in Anticancer Therapy*; IntechOpen: London, UK, 2018; p. 131.
61. Ul-Haq, I.; Ullah, N.; Bibi, G.; Kanwal, S.; Ahmad, M.S.; Mirza, B. Antioxidant and cytotoxic activities and phytochemical analysis of *Euphorbia wallichii* root extract and its fractions. *Iran. J. Pharm. Res. IJPR* **2012**, *11*, 241. [[PubMed](#)]
62. Khalil, A.T.; Ovais, M.; Ullah, I.; Ali, M.; Shinwari, Z.K.; Hassan, D.; Maaza, M. *Sageretia thea* (Osbeck.) modulated biosynthesis of NiO nanoparticles and their in vitro pharmacognostic, antioxidant and cytotoxic potential. *Artif. Cells Nanomed. Biotechnol.* **2018**, *46*, 838–852. [[CrossRef](#)] [[PubMed](#)]
63. Nasar, M.Q.; Khalil, A.T.; Ali, M.; Shah, M.; Ayaz, M.; Shinwari, Z.K. Phytochemical analysis, *Ephedra Procera* CA Mey. Mediated green synthesis of silver nanoparticles, their cytotoxic and antimicrobial potentials. *Medicina* **2019**, *55*, 369. [[CrossRef](#)]
64. Iravani, S.; Korbekandi, H.; Mirmohammadi, S.V.; Zolfaghari, B. Synthesis of silver nanoparticles: Chemical, physical and biological methods. *Res. Pharm. Sci.* **2014**, *9*, 385. [[PubMed](#)]

65. Vijayan, S.R.; Santhiyagu, P.; Ramasamy, R.; Arivalagan, P.; Kumar, G.; Ethiraj, K.; Ramaswamy, B.R. Seaweeds: A resource for marine bionanotechnology. *Enzym. Microb. Technol.* **2016**, *95*, 45–57. [[CrossRef](#)] [[PubMed](#)]
66. Jain, D.; Daima, H.K.; Kachhwaha, S.; Kothari, S. Synthesis of plant-mediated silver nanoparticles using papaya fruit extract and evaluation of their anti microbial activities. *Dig. J. Nanomater. Biostruct.* **2009**, *4*, 557–563.
67. Zhang, T.; Ye, J.; Xue, C.; Wang, Y.; Liao, W.; Mao, L.; Yuan, M.; Lian, S. Structural characteristics and bioactive properties of a novel polysaccharide from *Flammulina velutipes*. *Carbohydr. Polym.* **2018**, *197*, 147–156. [[CrossRef](#)] [[PubMed](#)]
68. Xiu, Z.M.; Zhang, Q.B.; Puppala, H.L.; Colvin, V.L.; Alvarez, P.J. Negligible particle-specific antibacterial activity of silver nanoparticles. *Nano Lett.* **2012**, *12*, 4271–4275. [[CrossRef](#)] [[PubMed](#)]
69. Ullah, R.; Shah, S.; Muhammad, Z.; Shah, S.A.; Faisal, S.; Khattak, U.; ul Haq, T.; Akbar, M.T. In vitro and in vivo applications of Euphorbia wallichii shoot extract-mediated gold nanospheres. *Green Process. Synth.* **2021**, *10*, 101–111. [[CrossRef](#)]
70. Faisal, S.; Khan, M.A.; Jan, H.; Shah, S.A.; Shah, S.; Rizwan, M.; Ullah, W.; Akbar, M.T. Edible mushroom (*Flammulina velutipes*) as biosource for silver nanoparticles: From synthesis to diverse biomedical and environmental applications. *Nanotechnology* **2020**, *32*, 065101. [[CrossRef](#)] [[PubMed](#)]
71. Nasr, H.; Nassar, O.; El-Sayed, M.; Kobisi, A. Characterization and antimicrobial activity of lemon peel mediated green synthesis of silver nanoparticles. *Int. J. Biol. Chem.* **2020**, *12*, 56–63. [[CrossRef](#)]
72. Bihari, P.; Vippola, M.; Schultes, S.; Praetner, M.; Khandoga, A.G.; Reichel, C.A.; Coester, C.; Tuomi, T.; Rehberg, M.; Krombach, F. Optimized dispersion of nanoparticles for biological in vitro and in vivo studies. *Part. Fibre Toxicol.* **2008**, *5*, 1–14. [[CrossRef](#)]
73. Modena, M.M.; Rühle, B.; Burg, T.P.; Wuttke, S. Nanoparticle characterization: What to measure? *Adv. Mater.* **2019**, *31*, 1901556. [[CrossRef](#)]
74. Jebali, A.; Kazemi, B. Nano-based antileishmanial agents: A toxicological study on nanoparticles for future treatment of cutaneous leishmaniasis. *Toxicol. In Vitro* **2013**, *27*, 1896–1904. [[CrossRef](#)]
75. Ratan, Z.A.; Haidere, M.F.; Nurunnabi, M.; Shahriar, S.M.; Ahammad, A.; Shim, Y.Y.; Reaney, M.J.; Cho, J.Y. Green chemistry synthesis of silver nanoparticles and their potential anticancer effects. *Cancers* **2020**, *12*, 855. [[CrossRef](#)]
76. Shah, S.; Shah, S.A.; Faisal, S.; Khan, A.; Ullah, R.; Ali, N.; Bilal, M. Engineering novel gold nanoparticles using Sageretia thea leaf extract and evaluation of their biological activities. *J. Nanostruct. Chem.* **2021**, 1–12. [[CrossRef](#)]
77. Suresh, J.; Yuvakkumar, R.; Sundrarajan, M.; Hong, S.I. Green Synthesis of Magnesium Oxide Nanoparticles. In *Advanced Materials Research*; Trans Tech Publications Ltd.: Freienbach, Switzerland, 2014; pp. 141–144.
78. Shah, R.; Shah, S.A.; Shah, S.; Faisal, S.; Ullah, F. Green Synthesis and Antibacterial Activity of Gold Nanoparticles of *Digera muricata*. *Indian J. Pharm. Sci.* **2020**, *82*, 374–378. [[CrossRef](#)]
79. Barzinjy, A.; Mustafa, S.; Ismael, H. Characterization of ZnO NPs prepared from green synthesis using Euphorbia Petiolata leaves. *EJSE* **2019**, *4*, 74–83.
80. Morais, M.; Namouni, F. Asteroids in retrograde resonance with Jupiter and Saturn. *Mon. Not. R. Astron. Soc. Lett.* **2013**, *436*, L30–L34. [[CrossRef](#)]
81. Shah, M.; Nawaz, S.; Jan, H.; Uddin, N.; Ali, A.; Anjum, S.; Giglioli-Guivarc'h, N.; Hano, C.; Abbasi, B.H. Synthesis of bio-mediated silver nanoparticles from *Silybum marianum* and their biological and clinical activities. *Mater. Sci. Eng. C* **2020**, *112*, 110889. [[CrossRef](#)] [[PubMed](#)]
82. Imran, M.; Jan, H.; Faisal, S.; Shah, S.A.; Shah, S.; Khan, M.N.; Akbar, M.T.; Rizwan, M.; Jan, F.; Syed, S. In vitro Examination of Anti-parasitic, Anti-Alzheimer, Insecticidal and Cytotoxic Potential of Ajuaga Bracteosa Wallich Leaves Extracts. *Saudi J. Biol. Sci.* **2021**, *28*, 3031–3036. [[CrossRef](#)]
83. Faisal, S.; Faisal, S.; Jan, H.; Shah, S.A.; Shah, S.; Khan, A.; Akbar, M.T.; Rizwan, M.; Jan, F.; Akhtar, N.; et al. (2021) Green Synthesis of Zinc Oxide (ZnO) Nanoparticles Using Aqueous Fruit Extracts of Myristica fragrans: Their Characterizations and Biological and Environmental Applications. *ACS Omega* **2021**, *14*, 9709–9722. [[CrossRef](#)] [[PubMed](#)]
84. Kainat; Khan, M.A.; Ali, F.; Faisal, S.; Rizwan, M.; Hussain, Z.; Zaman, N.; Afsheen, Z.; Uddin, M.N.; Bibi, N. Exploring the therapeutic potential of Hibiscus rosa sinensis synthesized cobalt oxide (Co<sub>3</sub>O<sub>4</sub>-NPs) and magnesium oxide nanoparticles (MgO-NPs). *Saudi J. Biol. Sci.* **2021**. [[CrossRef](#)]
85. Faisal, S.; Shah, S.A.; Shah, S.; Akbar, M.T.; Jan, F.; Haq, I.; Baber, M.E.; Aman, K.; Zahir, F.; Bibi, F.; et al. In Vitro Biomedical and Photo-Catalytic Application of Bio-Inspired *Zingiber officinale* Mediated Silver Nanoparticles. *J. Biomed. Nanotechnol.* **2020**, *16*, 492–504. [[CrossRef](#)]